Applied Surface Science xxx (2016) xxx–xxx

Contents lists available at ScienceDirect

Applied Surface Science

journal homepage: www.elsevier.com/locate/apsusc

Full Length Article

Ellipsometric study of the optical response of ZnS:Cr for PV applications

Thomas Brakstad[a,*], Benjamin R. Hope[a], Mohammadreza Nematollahi[a], Morten Kildemo[a], Nikolas J. Podraza[b], Kiran Ghimire[b], Turid W. Reenaas[a]

[a] Norwegian University of Science and Technology (NTNU), 7491 Trondheim, Norway
[b] University of Toledo, 2600 Dorr St., Toledo, OH 43606, USA

ARTICLE INFO

Article history:
Received 31 July 2016
Received in revised form 23 October 2016
Accepted 24 October 2016
Available online xxx

Keywords:
Ellipsometry
Cr doped ZnS
ZnS
Dielectric function

ABSTRACT

Optical properties of highly chromium doped (2–4 at.%) zinc sulfide made by pulsed laser deposition have been studied by spectroscopic ellipsometry in the spectral range of 0.73–5.90 eV. The characteristic optical features of the ZnS are a direct bandgap with absorption onset at 3.6 eV, with E_0, E_1 and E_2 critical points around 3.7, 5.7 and 7 eV. Excitonic effects were observed to be strong in this material – in line with the literature. The sub-bandgap absorption accredited to the chromium doping appears as a broad sub-bandgap feature increasing monotonously with increased doping concentration at a given growth temperature. In this report, we discuss three different approaches to extract and analyze the optical properties in terms of the complex dielectric function.

1. Introduction

An intermediate band solar cell (IBSC) is based on a semiconductor where a narrow, intermediate energy band (IB) is present within the bandgap (E_g) [1]. This additional band allows for better utilization of both low and high energy photons in the solar spectrum, as sub-bandgap light can excite electrons from the valence band (VB) to the IB and from the IB to the conduction band (CB). This increases the photo-generated current while maintaining a high open circuit voltage. The maximum theoretical efficiency (for fully concentrated light) of such a solar cell is as high as 63.2%, in comparison to a limit of 40.7% for a conventional solar cell under the same operating conditions [1]. Different approaches have been pursued, but the challenge remains to fabricate an IB material with suitable properties to obtain an IBSC with higher efficiency than a conventional solar cell [2].

ZnS is a well-studied and abundant material, which is interesting with regards to IBSC application. This is due to 1), an isolated, partially filled IB has been predicted by ab initio studies of Cr-doped ZnS [3,4], and 2), ZnS has a very large bandgap, (E_g ~3.6–3.9 eV) [5], which would make it easier to create an isolated IB within the bandgap with its own quasi-fermi level (QFL) when the solar cell is illuminated.

Undoped ZnS have been studied earlier using spectroscopic ellipsometry (SE), to obtain the optical constants of both zinc blende (ZB) [6,7] and wurtzite (WZ) [8] crystal structures. Doped ZnS has also been studied for various dopants, but only a few reports are found on ZnS:Cr [9,10] and none for very high dopant concentrations (2–4 at.%) which is needed for suppressing non-radiative recombination [11]. The complex dielectric function ($\varepsilon = \varepsilon_1 + i\varepsilon_2$) gives information on the material's electronic band structure, density of filled and empty states, magnitude of optical probability of a transition between filled and empty states, and excitonic absorption [12], and is therefore a highly important property to characterize.

In this work, we discuss three different approaches to model ε from room temperature ex situ spectroscopic ellipsometric data. Of particular importance is to understand how the Cr doping alters the dielectric function below the ZnS bandgap. Three different models for the optical response were applied, and these are presented below.

2. Experimental details

The ZnS and ZnS:Cr films were grown by pulsed laser deposition (PLD) on Si and quartz substrates. Prior to depositions, the substrates were cleaned using acetone, isopropanol, and deionized water. The Si substrates were etched in 5% HF for 3 min followed by 3 min rinsing in deionized water, and annealing at 850 C for 2 min in the PLD chamber. Then, the substrate temperature was reduced

* Corresponding author.
E-mail address: thomas.brakstad@ntnu.no (T. Brakstad).

http://dx.doi.org/10.1016/j.apsusc.2016.10.157
0169-4332/

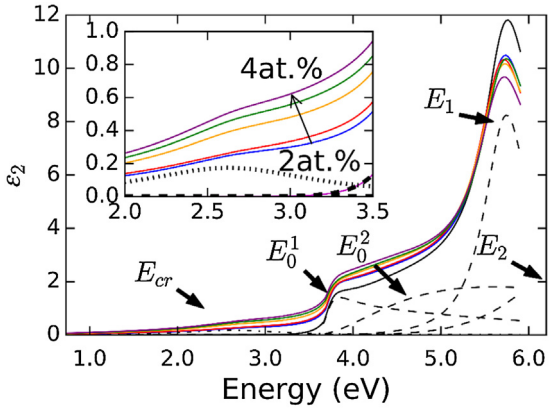

Fig. 1. ε_2 plotted for undoped (black) and different at.% of Cr (blue, red, orange, green and purple for 2.0, 2.3, 3.0, 3.3, and 4.0 at.%, respectively) ZnS films. The resulting lineshape from each oscillator for undoped ZnS is plotted in black, dashed lines, while the contribution for 4.0 at.% of the doped samples (black, dash-dotted line) are given as an example of below bandgap contribution. (For interpretation of the references to color in this figure legend, the reader is referred to the web version of this article.)

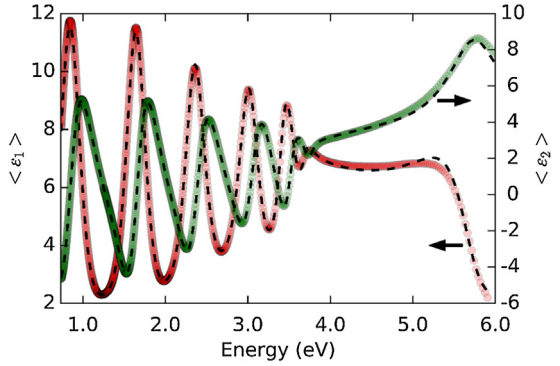

Fig. 2. The as-measured (colored circles) and simulated (black dotted lines) complex pseudo dielectric function (<ε>) for 4 at.% Cr-doped ZnS film. <ε_1> is plotted in red, while <ε_2> is plotted in green. The arrows indicate the corresponding axis. (For interpretation of the references to color in this figure legend, the reader is referred to the web version of this article.)

to the growth temperature, i.e. 500 C and 550 C for undoped and doped films, respectively. A KrF excimer laser (Lambda Physics COMPex Pro 110, 248 nm, 20 ns) was operated at 5 Hz to ablate a polycrystalline $(ZnS)_{0.94}Cr_{0.06}$ target. The Cr content in the films was varied between 2 and 4 at.% by varying the laser fluence in the range 1.0–4.3 J/cm^2 as elaborated in Ref. [13]. The films were between 160 and 660 nm thick [14].

The optical properties of the films were determined using a dual rotating compensator variable angle spectroscopic ellipsometry (VASE) (RC2, J.A. Woollam Co.) in the wavelength range 210–1690 nm (photon energy range 0.73–5.90 eV). Spectra were recorded at incidence angles of 60–75°, with 2.5° increments. In addition, VUV-VASE was used for measurements of selected samples in the 4.0–8.5 eV range.

3. Results and discussion

3.1. Modeling details

All ZnS layers were modelled as a homogeneous thin film on a semi-infinite c-Si substrate covered by a native oxide. A simple Bruggeman effective medium approximation (BEMA) consisting of 50/50 void/ZnS for the undoped samples, and void/ZnS:Cr for the doped samples, was used to model the surface roughness [15]. Surface roughness's were compared to atomic force microscopy (AFM) measurements from Ref. [16], and the films were in general found to be very smooth, with root mean squared roughness values of 1.2–2.8 nm [16]. The roughness, native oxide and ZnS layer thicknesses were all fitted. The agreement between the optical model and the measured ellipsometric spectra (in $N = \cos 2\Psi$, $C = \sin 2\Psi \cos\Delta$, $S = \sin 2\Psi \sin\Delta$) was quantified by the mean squared error (MSE) [17].

3.2. Harmonic oscillator dispersion model

In this approach, the main features of the ZnS layer was modelled by one Cody-Lorentz oscillator with an Urbach tail (labeled E_0^1 in Fig. 1) corresponding to a 3D exciton (according to Ozaki and Adachi [6]), and a Tauc Lorentz oscillator (E_1) modelling the E_1−CP, which is dominated by an exciton. The model was refined to include one Tauc Lorentz oscillator (E_0^2 in Fig. 1), which resembles the E0/E0 + Δ critical point found by Ozaki and Adachi. The two Tauc Lorentz oscillators used the same bandgap value (E_g). Indeed, this was motivated by Ozaki and Adachi [6] dispersion model describing the absorption at the bandgap edge by a combination of an exciton lineshape and a 3D-CP. The E_2−CP and other high energy transitions were grouped into a Gaussian oscillator, (mainly from the E_2−CP around 7 eV). These lineshape-components are shown in Fig. 1 (black dashed lines), along with the resulting imaginary part of the dielectric function (full black line). The other, colored curves above the black lineshape is ε_2 for various amount of Cr in the ZnS films ranging from 2.0 to 4.0 at.% Cr.

Table 1
Parameters for the harmonic oscillator model as a function of Cr content. E_g was here 3.56 eV and $\varepsilon_\infty = 1$. The Cody Lorentz parameters were $E_p = 3.0$, $E_t = 0.109$ and $E_u = 0.129$ eV. Broadening and the position of the E_{cr} Lorentzian oscillator was set to $\Gamma_{Cr} = 0.85$ and $E_{cr} = 2.68$ eV. E_1 is the position for the center of oscillator, A_1 is the amplitude, Γ_1 is the broadening, and A_{cr} is the amplitude of the Cr contribution.

	ZnS	2.0 at.%	2.3 at.%	3.0 at.%	3.3 at.%	4.0 at.%
E_1 (eV)	5.73	5.70	5.68	5.69	5.71	5.68
A_1	36.50	32.37	32.41	32.02	30.93	29.06
Γ_1 (eV)	0.54	0.66	0.67	0.69	0.66	0.68
A_{cr}	N/A	0.06	0.04	0.08	0.09	0.10

The as-measured pseudo dielectric function of a typical doped ZnS film is shown in Fig. 2. We note the sharp cut-off of the interference fringes at the bandgap, around 3.7 eV related to the E_0−CP, and the strong feature around 5.7 eV related to the E_1−CP.

The E_0^1 shape in our model is much broader than the excitonic peak in the Ozaki and Adachi model [6]. The E_1 peak was for simplicity modelled by a Tauc-Lorentz oscillator, rather than an exciton lineshape, in order to insure cut-off at the bandgap.

To account for new states in the bandgap when doping ZnS with Cr, one Lorenz oscillator, with center energy (E_{Cr}) was added to account for the increased absorption below the bandgap. The lineshape contribution for 4 at.% Cr is seen in Fig. 1, and the complete model shows a good agreement with the data, as exemplified in Fig. 2. The large number of parameters was compensated for by performing a multi sample analysis of all samples, and some main parameters are shown in Table 1.

The E_1 amplitude in Fig. 1 is reduced significantly for 4 at.% of Cr compared to the undoped sample. Between 2.0% and 3.3% doping content, the E_1 peak is only slightly reduced or not reduced at all. The peak amplitude of the E_1 peak is reduced following the introduction of doping, but no significant change in its energy position or the broadening of the peak can be seen from Fig. 1 or Table 1.

Please cite this article in press as: T. Brakstad, et al., Ellipsometric study of the optical response of ZnS:Cr for PV applications, Appl. Surf. Sci. (2016), http://dx.doi.org/10.1016/j.apsusc.2016.10.157

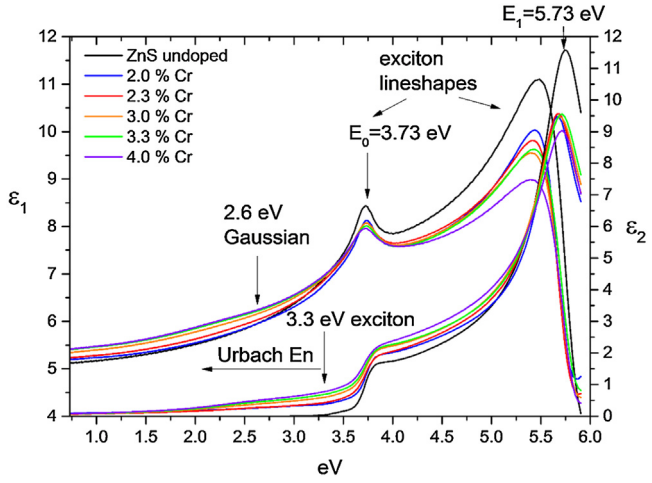

Fig. 3. Dielectric functions determined using the numerical CPPB model modified by the Urbach tail. Black, blue, red, orange, green, and purple for undoped ZnS, 2.0, 2.3, 3.0, 3.3, and 4.0 at.% Cr content, respectively. (For interpretation of the references to color in this figure legend, the reader is referred to the web version of this article.)

3.3. CPPB dispersion model modified by an Urbach tail

A model which incorporates critical point parabolic band (CPPB) dispersion for all the CPs, but which falls off sufficiently fast in order to correctly model the interference fringes and the weak sub-bandgap absorption, as in Figs. 2 and 4, has recently been proposed [18]. The idea is that the below bandgap absorption tail of the CPs are multiplied by the Urbach tail, as in the Tauc-Lorentz model [19,20]. In our implementation the dispersion model is described by:

$$\varepsilon_1(E) = \varepsilon_\infty + \frac{A}{E_{res}^2 - E^2} + \frac{2}{\pi} P \int_0^\infty \frac{\zeta \varepsilon_2(\zeta)}{\zeta^2 - E^2} d\zeta, \quad (1)$$

where the imaginary part is for simplicity given by the sum of only exciton line shapes:

$$\varepsilon_2(\mathrm{E}) = \begin{cases} \varepsilon_{2,Gauss}(E) + \varepsilon_{2,CPPB}\left(E_g\right) e^{-\frac{(E_g - E)}{E_u}}, & E < E_g \\ \varepsilon_{2,Gauss}(E) + \varepsilon_{2,CPPB}(\mathrm{E}), & E \geq E_g \end{cases} \quad (2)$$

$$\varepsilon_{2,CPPB}(E) = \sum_{q=1}^{4} \mathrm{Im}\left[A_q e^{i\phi} \left(\frac{\Gamma_q}{2E_q - 2E - i\Gamma_q} \right)^{\mu_q} \right] \quad (3)$$

Here, A is the amplitude, E_q is the CP energy, Γ_q is the broadening, μ_q is the dimensionality of the CP, and φ is the phase. E_{res} in the second term in Eq. (1) is the resonance energy outside the range of measurement. The resulting ε is shown in Fig. 3, and shows the same features and trends as the parametric dispersion model. The modified CPPB dispersion model also gave an excellent fit to the data from undoped to 4% Cr doped ZnS (see Fig. 4), and appeared reasonably stable. That is, the weak Gaussian sub-band absorption was only added at the very end of the fit, and only the two highest doping ratios showed a major improvement in MSE (factor 2 for these samples). Note that the Sellmeier function (i.e. the second term in Eq. (1)) was not needed if a sufficient number of oscillators were added in the UV and the corresponding Kramers-Kronig (KK) integral performed up to at least 9 eV. Such oscillators could be estimated from VUV-ellipsometry data.

The parametric fit, with all CPs limited to $\mu = 1$, i.e. excitonic line shapes, gave all reasonable fits without the Gaussian inter-band, implying that the long absorption tail describes the main absorption. However, adding the Gaussian sub-band absorption reduced the final MSE by a factor 2 for the highest doping levels, see Fig. 4. Typical parameters are shown in Table 2. It is observed that the Urbach energy was found to be around 1.2 eV which basically allows for the long tail of the absorption towards lower energies, while the Gaussian is located near 2.57 eV. The advantage of the latter model is that it allows to determine accurate values for the E_0–CP, to describe the range of states through the Urbach tail, and to describe the weak localized states that have features similar to Cr^{2+} photoionization at around 2.8 eV [21].

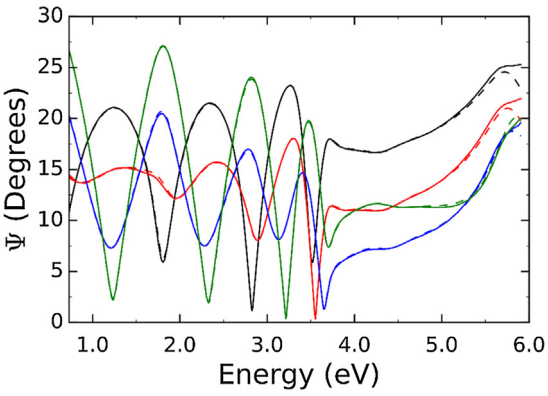

Fig. 4. The ellipsometric parameter Ψ at angles of incidences $\theta_0 = 60$ (black), 65 (red), 70 (blue) and 75 (green) degrees, for 3.3 at.% of Cr doped ZnS. The full lines correspond to the experimental data, and the dotted lines are the CPPB dispersion model fit. (For interpretation of the references to color in this figure legend, the reader is referred to the web version of this article.)

Table 2
Selected parameters used in the CPPB dispersion model for E_g equal to 3.36 eV and ε_∞ varied from 1 to 1.3. The Urbach energy varied from $E_u = 1.1$–1.3 eV. Broadening and the position of the E_{cr} Gaussian oscillator was set to $\Gamma = 0.80 \pm 0.1$ and $E_{cr} = 2.56 \pm 0.01$ eV E_1 is the position for the center of oscillator, A is the amplitude, Γ is the broadening, and A_{cr} is the amplitude of the Cr contribution.

	ZnS	2.0 at.%	2.3 at.%	3.0 at.%	3.3 at.%	4.0 at.%
E_1 (eV)	5.8	5.7	5.7	5.7	5.7	5.8
A_1	8.35	5.80	5.84	5.83	5.80	5.47
Γ_1 (eV)	0.54	0.46	0.50	0.54	0.53	0.52
A_{cr}	N/A	0.02	0.02	0.06	0.07	0.08

Table 3
The position, E_1, broadening, Γ_1, and amplitude, A_1, for the ZnS film and 2–4 at.% Cr doped ZnS samples for the 2nd derivative analysis.

	ZnS	2.0 at.%	2.3 at.%	3.0 at.%	3.3 at.%	4.0 at.%
E_1	5.73	5.71	5.72	5.73	5.74	5.74
A_1	2.61	3.00	3.19	2.94	2.61	2.25
Γ_1	0.32	0.39	0.42	0.41	0.38	0.37

3.4. Direct inversion and 2nd derivative CPPB analysis

The dielectric function was extracted with the KK-consistent B-spline method [22]. The double derivatives for the PLD series after smoothening are plotted in Fig. 5. The main changes of the double derivatives as a function of doping concentration have been marked with black arrows. When the doping level increases, it is seen that the E_0 feature at 3.7 eV becomes weaker, more broadened but do not change much in energy, while the E_1 feature at around 5.7 eV becomes less broadened and shifts to higher energy.

Some key CP lineshape parameters from the fit to the 2nd derivative of the undoped pulsed laser deposited sample are given in Table 3. The fit of the undoped sample was used as a starting point for the analysis of the doped samples, and a comparison of the prin-

Please cite this article in press as: T. Brakstad, et al., Ellipsometric study of the optical response of ZnS:Cr for PV applications, Appl. Surf. Sci. (2016), http://dx.doi.org/10.1016/j.apsusc.2016.10.157

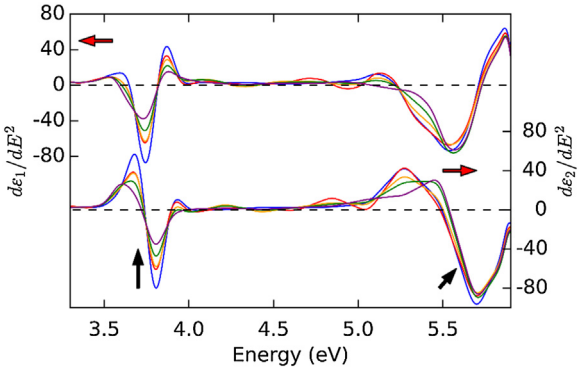

Fig. 5. The double derivatives of the dielectric function for ZnS:Cr. Blue, red, orange, green, and purple for 2.0, 2.3, 3.0, 3.3, and 4.0 at.% Cr, respectively. The red arrow indicate the graph's axis, while the black arrows indicate the trend for increasing Cr at.%. (For interpretation of the references to color in this figure legend, the reader is referred to the web version of this article.)

Table 4
The E_0^1, E_0^2, E_1 and E_2 position, in eV, from the general oscillator model, modified critical point parabolic band model, 2nd derivative analysis (2da) of ε_2 from the B-spline model, as well as values from the literature [6,7] for undoped ZnS.

	Gen. Osc.	Modified CPPB	2da (B-spline)	Ozaki and Adachi [6]	Ghong et al. [7]
E_0^1	3.69	3.34	3.75	3.75	
E_0^2	3.73	3.72	3.78	3.82	
E_1	5.73	5.76	5.73	5.74	5.85
E_2	7.30	7.24	7.00	7.00	7.03

cipal parameters, E_0^1, E_0^2 and E_1 CPs, are shown in Table 4. The CP energies are in overall agreement with the energies extracted by the CPPB model in Ref. [6]. Note that two nearly superposing CPs (one excitonic ($\mu = 1$) and one 3D-M_0 ($\mu = 0.5$, $\varphi = 280$, $E_0 \sim 3.75$ eV)) were found to fit the 2nd derivate spectra, while the CPPB dispersion model systematically rather converged to a single exciton lineshape at 3.73 eV, and a more curious broader lineshape below the E_0 gap (around 3.34 eV).

One hypothesis regarding the crystal structure of the ZnS films was that the original ZnS were mostly ZB phase, while the WZ fraction increased with increasing Cr-content. This was difficult to confirm with XRD measurements as the WZ and ZB peaks overlap [13]. By analyzing the position and amplitude of the E_1 peak, it can be seen that the amplitude diminishes, indicating that the WZ fraction might increase (see Table 3). However, the position of the E_1 peak does not seem to change as one might expect for increasing WZ [8], making the crystal phase purity another possible cause for the broadening and diminishing amplitude for the E_1 peak. Measurements of pure WZ phase ZnS is needed to test this hypothesis.

In order to quantify sub-bandgap absorption as a function of Cr concentration, we estimated the transition strength, f, from the B-spline extracted imaginary part of the dielectric function [22], giving: $f(E) = M \int_{E_1}^{E_2} \varepsilon_2(E) E dE$. The transition strength gave similar results for all dispersion models, and it displays a linear relationship between transition strength and Cr content, indicating that the increase in sub-band absorption is due to increased Cr doping. This relationship was also found and plotted in Ref. [14].

4. Summary and conclusions

Two parametric dispersion models were applied in order to describe undoped ZnS; a harmonic oscillator based model (Cody Lorentz) and a modified CPPB model. By appropriate modelling of the dielectric function, we were able to extract weak sub-bandgap absorption of ZnS:Cr, potentially related to an intermediate band. The parameters of these models were compared to the result of the 2nd derivative analysis (also using CPPB line shapes) of B-spline extracted dielectric function of the films.

The harmonic based model does not in principle convey the details of the CPs (type, dimension etc.), and also consisted of a large number of free parameters. This issue was resolved by using a modified CPPB model, which still allowed for the sharp cut-off at the E_0 gap to be accurately modelled.

As excitonic absorption dominates for ZnS and similar wide bandgap semiconductors, therefore both approaches probably fit equally well, and explains the similar position of the CPs. Finally these CP positions are in good correspondence with those determined using line shape fitting of 2nd derivative spectra of the B-spline extracted dielectric function.

Acknowledgments

This work was performed with partial support from the Norwegian Center for Solar Cell Technology (project 193829) and the Norwegian Research Council (grants 240466 and 221860/F60).

References

[1] A. Luque, A. Marti, Increasing the efficiency of ideal solar cells by photon induced transitions at intermediate levels, Phys. Rev. Lett. 78 (1997) 5014–5017, http://dx.doi.org/10.1103/PhysRevLett.78.5014.
[2] A. Datas, E. López, I. Ramiro, E. Antolín, A. Martí, A. Luque, Intermediate band solar cell with extreme broadband spectrum quantum efficiency, Phys. Rev. Lett. 114 (2015) 1–4, http://dx.doi.org/10.1103/PhysRevLett.114.157701.
[3] C. Tablero, Optoelectronic properties of Cr-substituted II–VI semiconductors, Comput. Mater. Sci. 37 (2006) 483–490, http://dx.doi.org/10.1016/j.commatsci.2005.11.009.
[4] C. Tablero, Effects of the impurity-host interactions on the nonradiative processes in ZnS:Cr, J. Appl. Phys. 108 (2010) 93114, http://dx.doi.org/10.1063/1.3506705.
[5] Collaboration: Authors and editors of the volumes III/17B-22A-41B, Zinc Sulfide (ZnS) Band Structure, Cubic Modification, in: O. Madelung, U. Rössler, M. Schulz (Eds.), Springer Materials–The Landolt–Börnstein Database, 2014 http://www.springermaterials.com.
[6] S. Ozaki, S. Adachi, Optical constants of cubic ZnS, Jpn. J. Appl. Phys. 32 (1993) 5008–5013, http://dx.doi.org/10.1143/jjap.32.5008.
[7] T.H. Ghong, T.J. Kim, Y.D. Kim, Study of the dielectric function of ZnS by spectroscopic ellipsometry, J. Korean Phys. Soc. 42 (2003) 238–241.
[8] J.L. Freeouf, Far-ultraviolet reflectance of II–VI compounds and correlation with the Penn—Phillips gap, Phys. Rev. B 7 (1973) 3810–3830, http://dx.doi.org/10.1103/physrevb.7.3810.
[9] K. Ichino, Y. Morimoto, H. Kobayashi, Molecular beam epitaxy and structural properties of ZnCrS, Phys. Status Solidi 3 (2006) 776–779, http://dx.doi.org/10.1002/pssc.200564699.
[10] M.P. Sarma, G. Wary, Structural and optical properties of nanocrystalline pb1-xCdxS thin films prepared by chemical bath deposition, Am. J. Mater. Sci. Technol. 4 (2015) 58–71, http://dx.doi.org/10.5539/apr.v4n3p75.
[11] A. Luque, A. Martí, E. Antolín, C. Tablero, Intermediate bands versus levels in non-radiative recombination, Phys. B Condens. Matter 382 (2006) 320–327, http://dx.doi.org/10.1016/j.physb.2006.03.006.
[12] H. Tompkins, E. Irene, Handbook of Ellipsometry, Elsevier Inc., 2005, http://dx.doi.org/10.1007/3-540-27488-x.
[13] M. Nematollahi, X. Yang, U.J. Gibson, T.W. Reenaas, Pulsed laser ablation and deposition of ZnS:Cr, Thin Solid Films 590 (2015) 28–32, http://dx.doi.org/10.1016/j.tsf.2015.07.046.
[14] M. Nematollahi, X. Yang, L.M.S. Aas, Z. Ghadyani, M. Kildemo, U.J. Gibson, T.W. Reenaas, Molecular beam and pulsed laser deposition of ZnS:Cr for intermediate band solar cells, Sol. Energy Mater. Sol. Cells 141 (2015) 322–330, http://dx.doi.org/10.1016/j.solmat.2015.06.004.
[15] H. Fujiwara, J. Koh, P. Rovira, R. Collins, Assessment of effective-medium theories in the analysis of nucleation and microscopic surface roughness evolution for semiconductor thin films, Phys. Rev. B 61 (2000) 10832–10844, http://dx.doi.org/10.1103/PhysRevB.61.10832.
[16] M. Nematollahi, X. Yang, E. Seim, P.E. Vullum, R. Holmestad, U.J. Gibson, T.W. Reenaas, Compositional and structural properties of pulsed laser-deposited ZnS:Cr films, Appl. Phys. A 122 (2016) 1–11, http://dx.doi.org/10.1007/s00339-016-9594-9.
[17] B. Johs, C.M. Herzinger, Quantifying the accuracy of ellipsometer systems, Phys. Status Solidi 5 (2008) 1031–1035, http://dx.doi.org/10.1002/pssc.200777755.

[18] K. Ghimire, H.F. Haneef, R.W. Collins, N.J. Podraza, Optical properties of single-crystal Gd3Ga5O12 from the infrared to ultraviolet, Phys. Status Solidi 252 (2015) 2191–2198, http://dx.doi.org/10.1002/pssb.201552115.
[19] J. Tauc, R. Grigorovici, A. Vancu, Optical properties and electronic structure of amorphous germanium, Phys. Status Solidi 15 (1966) 627, http://dx.doi.org/10.1002/pssb.19660150224.
[20] G.E. Jellison Jr., F.A. Modine, Parameterization of the optical functions of amorphous materials in the interband region, Appl. Phys. Lett. 69 (1996) 371–373, http://dx.doi.org/10.1063/1.118064.
[21] N.A. Vlasenko, P.F. Oleksenko, Z.L. Denisova, M.O. Mukhlyo, L.I. Veligura, Cr-related energy levels and mechanism of Cr2+ ion photorecharge in ZnS:Cr, Phys. Status Solidi Basic Res. 245 (2008) 2550–2557, http://dx.doi.org/10.1002/pssb.200844044.
[22] W. Oldham, Numerical techniques for the analysis of lossy films, Surf. Sci. 16 (1969) 97–103, http://dx.doi.org/10.1016/0039-6028(69)90008-9.

Please cite this article in press as: T. Brakstad, et al., Ellipsometric study of the optical response of ZnS:Cr for PV applications, Appl. Surf. Sci. (2016), http://dx.doi.org/10.1016/j.apsusc.2016.10.157